CrossMark

Synthesis of whey peptide-iron complexes: Influence of using different iron precursor compounds

Maria Elisa Caetano-Silva[a], Renata Carolina Alves[b], Guilherme Nunes Lucena[b], Regina Célia Galvão Frem[b,*], Maria Teresa Bertoldo-Pacheco[c], Juliana Azevedo Lima-Pallone[a], Flavia Maria Netto[a,**]

[a] Faculty of Food Engineering, University of Campinas, UNICAMP, Monteiro Lobato 80, 13083-862 Campinas, SP, Brazil
[b] Institute of Chemistry, São Paulo State University, UNESP, Prof. Francisco Degni 55, PO Box 355, 14800-970 Araraquara, SP, Brazil
[c] Center of Food Science and Quality, Institute of Food Technology, ITAL, Brasil Ave 2880, 13070-178 Campinas, SP, Brazil

ARTICLE INFO

ABSTRACT

Iron-binding peptides are an alternative for increasing the bioavailability of iron and to decreasing its pro-oxidant effect. This study aimed to synthesize and characterize peptide-iron complexes using $FeCl_2$ or $FeSO_4$ as the iron precursor compounds. Whey protein isolate (WPI), WPI hydrolyzed with pancreatin, and its fractions obtained via ultrafiltration (cut-off 5 kDa) were used as ligands. The fluorescence intensity of the ligands significantly decreased as the iron concentration increased as a result of metal coordination with the iron-binding sites, which may have led to changes in the microenvironment of tryptophan. For both iron precursor compounds, the primary iron-binding site was carboxylate groups, and the linkage occurred via a bidentate coordination mode with two vibrational modes assigned to the COO−Fe linkage. However, infrared spectroscopy and thermal analysis results showed that the dynamics of the interaction is different for the iron precursor. The iron source may be of great importance because it may impact iron absorption and the pro-oxidant effect of the mineral.

1. Introduction

Iron is an essential micronutrient and an intrinsic component of hemoglobin, myoglobin, and cytochromes (Luo & Xie, 2012). This mineral acts as a regulator, activator, and controller of several enzymatic reactions. Among iron's functions, the formation of red blood cells, O_2 and CO_2 transport, electron transfer, redox reactions and cellular energy production can be highlighted (Lieu, Heiskala, Peterson, & Yang, 2001). Therefore, iron deficiency is responsible for several diseases and is one of the primary nutritional problems worldwide. Many efforts have been made to combat this deficiency, mainly regarding food fortification. However, this practice is still a challenge due to the questions associated, such as low bioavailability, digestive problems, such as stomach ache or diarrhea, and even changes in the flavor and appearance of food products (Sugiarto, Ye, & Singh, 2009).

Peptide-iron complexes can be an alternative to mitigate these problems. Under certain conditions, iron binding with an organic compound promotes the formation of complexes, which protects the micronutrient against the chemical reactions that occur during the digestive process (Gligic, Palic, & Nikolovski, 2004). Iron-peptide binding is based on the interaction between an electron donor group at the ligand surface (in this case, peptide) and a Lewis acid (transition metal ion). Peptides may present one or more accessible coordinating sites, ensuring that the metal atom becomes part of a biologically stable structure through coordinate covalent bonding. In this way, the complexed mineral is less prone to interactions with the chemical neighborhood (Miquel & Farré, 2007).

Ferrous or ferric salts, such as $FeCl_2$, $FeCl_3$, and $FeSO_4$, have been used to synthesize peptide-iron complexes and to study the iron-binding capacity of peptides (Caetano-Silva, Bertoldo-Pacheco, Paes-Leme, & Netto, 2015; Chaud et al., 2002; Huang, Ren, & Jiang, 2011; Kim et al., 2007; O'Loughlin, Kelly, Murray, FitzGerald, & Brodkorb, 2015; Ueno, Urazono, & Kobayashi, 2014; Zhou et al., 2012). Nevertheless, to the best of our knowledge, no effort has been made to study the effect of iron sources on complex formation, even though the role of different ions on peptide and protein structure and interactions is
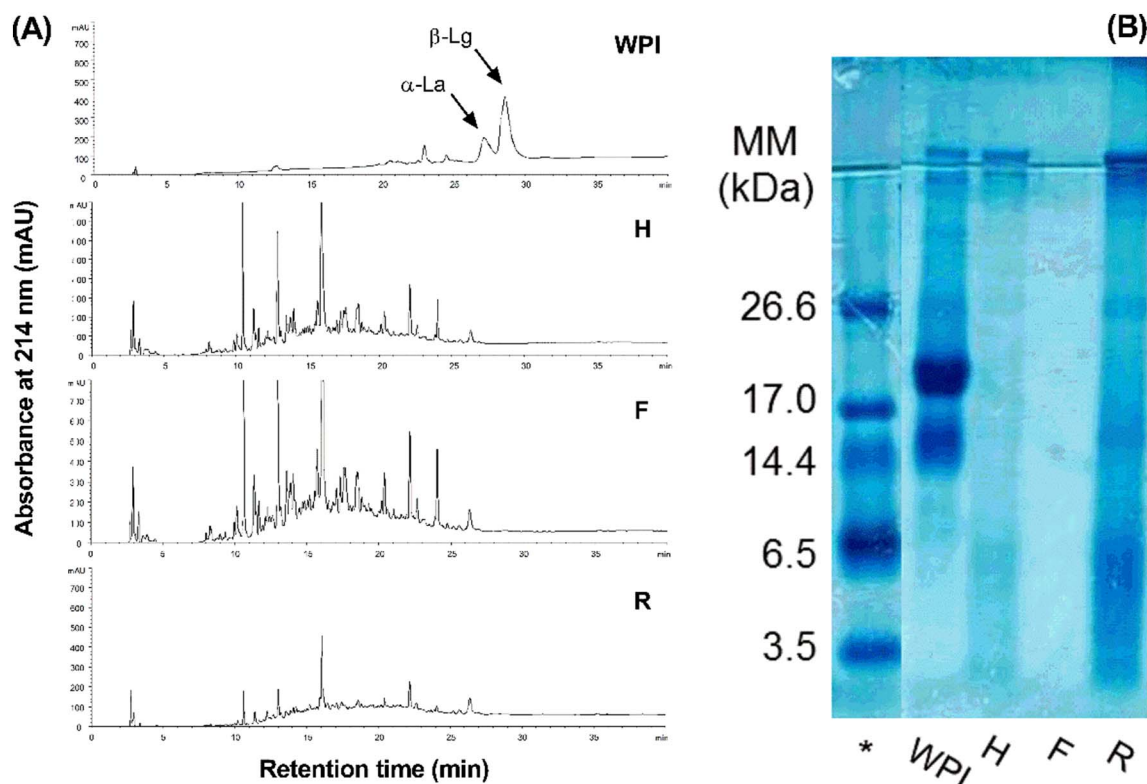

Fig. 1. (A) Chromatographic profile (RP-HPLC) and (B) electrophoretic profile (SDS-PAGE Tricine) of ligands. **WPI** – whey protein isolate; **H** - hydrolysate; **F** – filtrate (fraction < 5 kDa); **R** - retentate (fraction > 5 kDa). * Molecular mass standard.

widely known (Zhang & Cremer, 2006).

Our previous studies showed that fractions of WPI hydrolysate with pancreatin have the same iron-binding sites regardless of the molecular mass (MM) (Caetano-Silva et al., 2015); however, only complexes synthesized with low-MM peptides (MM < 5 kDa) showed a capacity to increase iron uptake in vitro compared with the iron salt form. Regarding the iron source, complexes synthesized with $FeCl_2$ led to greater ferritin synthesis than complexes synthesized with $FeSO_4$ (p < 0.05) (Caetano-Silva, Cilla, Bertoldo-Pacheco, Netto, & Alegría, 2017). Therefore, our results suggested that different iron precursors influence the functionality of the complexes due to differences in complex structure caused by the counter ions, chloride or sulfate. The aim of the present work was to test this hypothesis using peptide-iron complexes synthesized using two iron salts, $FeCl_2$ and $FeSO_4$, and different MM ligands to understand the effect of the iron source on the dynamics of the peptide-iron interaction, which may contribute to their future application for food fortification.

2. Materials and methods

2.1. Materials

Whey protein isolate (WPI) was obtained from Glanbia Nutritionals (Kilkenny, Ireland). Pancreatin (4xUSP, from porcine pancreas, EC 232-468-9, P1750) was purchased from Sigma-Aldrich® (St. Louis, MO, USA). Iron precursors, $FeCl_2 \cdot 4H_2O$ and $FeSO_4 \cdot 7H_2O$, were purchased from J.T. Baker (Phillipsburg, NJ, USA) and Sigma-Aldrich® (St. Louis, MO, USA), respectively. All other chemicals and reagents used were of analytical or chromatographic grade.

2.2. Preparation of hydrolysate and its fractions

The hydrolysate was obtained from enzymatic hydrolysis of WPI with the enzymatic system pancreatin under previously defined conditions (Caetano-Silva et al., 2015). Briefly, WPI was diluted in deionized water (10% protein w/v), and the reaction occurred at pH 8.0; it was monitored using an automatic titrator, pH Stat (Mettler-Toledo, model DL 21 Grafix, Schwerzenbach, Switzerland) with stirring and a controlled temperature (40 °C). After 180 min, the enzyme was deactivated by heating (85 °C for 15 min), and the reaction mixture was cooled in an ice bath.

The degree of hydrolysis (DH), determined according to Adler-Nissen (1986), was 16.2%. The pH was adjusted to 6.0 with 1 mol/L HCl, and a portion of the reaction mass was then freeze-dried; this sample was named hydrolysate (**H**). A portion of **H** was fractionated in a Pellicon® ultrafiltration system (Millipore, Bedford, MA, USA) with a cut-off membrane of 5 kDa (Cartridge Prep/Scale – TFF 6 ft²). The fraction with an MM < 5 kDa was named filtrate (**F**), and the one with MM > 5 kDa was named retentate (**R**).

2.3. Characterization of the ligands

2.3.1. Chromatography

Reversed-phase high-performance liquid chromatography (RP-HPLC) was performed in an Agilent liquid chromatograph with a semi-preparative and analytical quaternary pump system and a diode array detector (DAD) (Agilent, Waldbronn, Germany) on a Microsorb – MV™ C_{18} column (4.6 mm × 250 mm; 5 μm particle size) (Rainin, Woburn, MA, USA). The solvent composition was solvent A – 0.04% de TFA in ultrapure water; solvent B – 0.03% TFA in acetonitrile. The gradient elution conditions were solvent B from 0 to 70% in 40 min, 100% in 5 min, and returning to 0% in 5 more min. Detection was at 214 nm, and the sample injection volume was 50 μL (3 mg protein/mL for **H**, **F**, and **R**, and 1 mg protein/mL for **WPI**). The proteins, α-lactoalbumin (α-La) and β-lactoglobulin (β-Lg), from bovine milk (Sigma-Aldrich®, St. Louis, MO, USA), were used as standards.
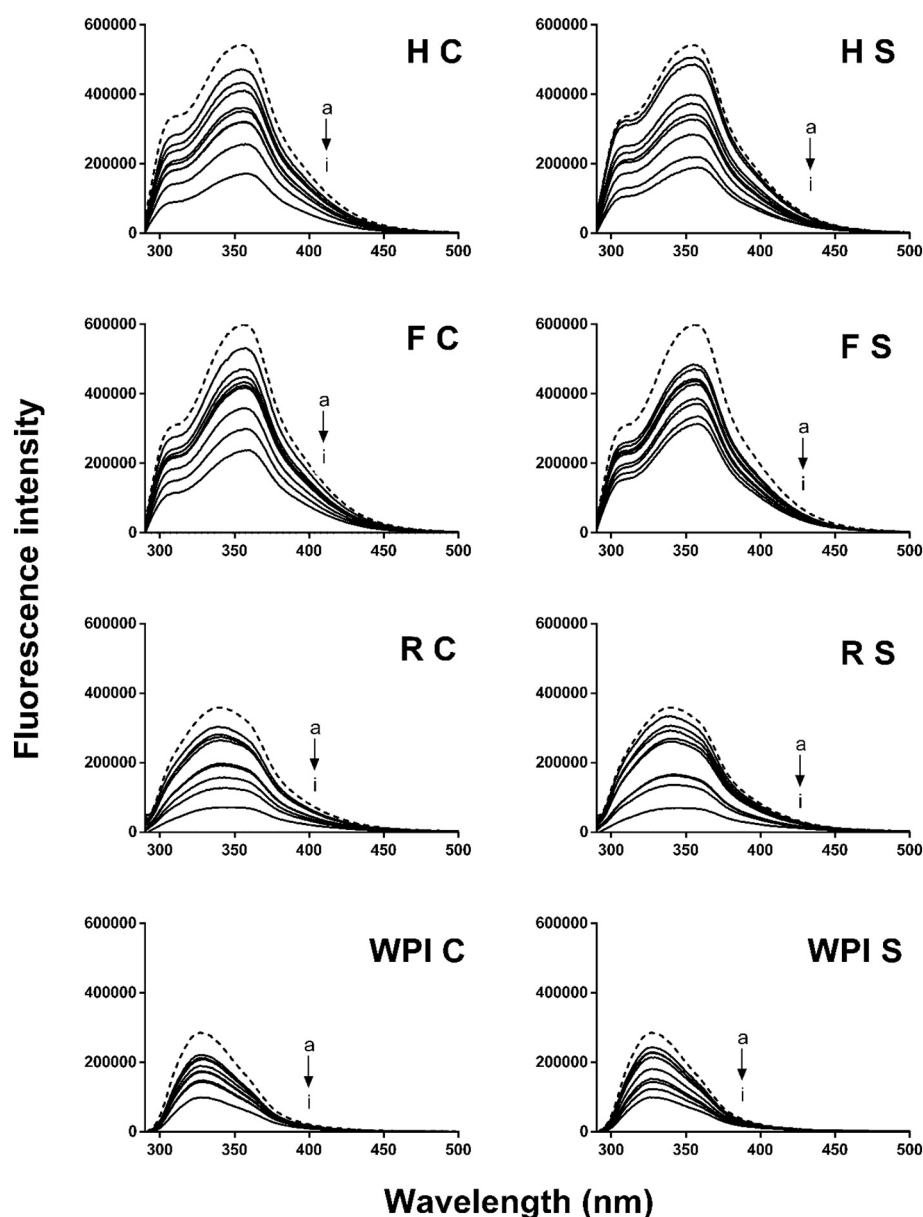
Fig. 2. Fluorescence emission spectra of ligands **H** - hydrolysate; **F** – filtrate (fraction < 5 kDa); **R** – retentate (fraction > 5 kDa); **WPI** – whey protein isolate (5 mg protein/mL) without iron addition (dashed lines) and with addition of **C** - $FeCl_2$ or **S** - $FeSO_4$ (full lines) in different iron:protein ratios. (a–i) 10; 20; 30; 40; 60; 80; 100; 200; 400 μmol Fe/g protein. Excitation wavelength: 280 nm; emission wavelength: 290–500 nm.
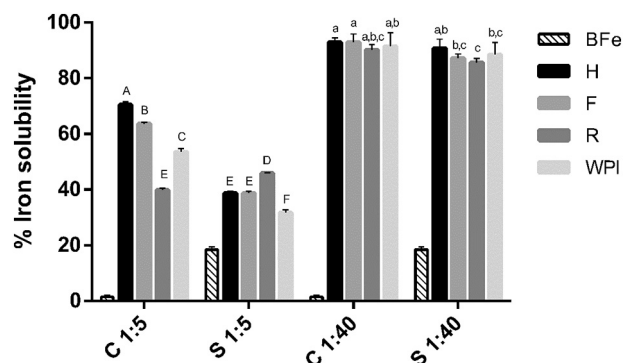

Fig. 3. Iron solubility (%) after complexes synthesis (pH 7.0) under ratio iron:protein (w/w) of 1:40 or 1:5 with $FeCl_2$ (**C**) or $FeSO_4$ (**S**). **BFe** - control assay with only iron salt; **H** - hydrolysate; **F** - filtrate (fraction < 5 kDa); **R** - retentate (fraction > 5 kDa); **WPI** - whey protein isolate. * samples with different letters are statistically different ($p < 0.05$); controls assays (**BFe C** e **BFe S**) are not included in the statistical analysis ANOVA and Tukey.

2.3.2. Electrophoresis

The electrophoretic profiles were obtained using the SDS-PAGE Tricine system according to Schagger (2006) with a separation gel containing 16% acrylamide and 6 mol/L urea and with resolving and stacking gels containing 10% and 4% of acrylamide, respectively. Ligands were diluted (1% protein w/v) in reducing buffer (0.5 mol/L Tris–HCl, pH 6.8, 10% SDS, 10% glycerol, 5% β-mercaptoethanol and 0.1% Coomassie Blue G250) and heated at 90 °C for 5 min. Aliquots of 10 μL of each sample were subsequently loaded onto the gels. The MM of the peptides was estimated using a 3.5–26 kDa marker kit (Bio-Rad, Hercules, CA, USA) as the standard.

2.4. Intrinsic fluorescence spectroscopy

Intrinsic fluorescence emission spectra of the ligands **H, F, R,** and **WPI** with the addition of different amounts of iron from $FeCl_2$ or $FeSO_4$ (0–2 mmol Fe/L) were obtained using a multifrequency phase ISS K2 fluorometer (Champaign, IL, USA). The excitation wavelength was 280 nm, and emission wavelengths ranging from 290 to 500 nm were recorded. To this end, stock solutions of iron salts (6 mmol Fe/L) and/

Table 1

Main absorption bands in the infrared and tentative assignments of the corresponding vibrational modes of free ligands (**H**, hydrolysate; **F**, filtrate; **R**, retentate and **WPI**, whey protein isolate) and their respective iron complexes, obtained from FeCl$_2$ (−**Fe C**) or FeSO$_4$ (−**Fe S**).

Sources for assignment to vibrational modes: (Acevedo-Chávez, Costas, Bernès, Medina, & Gasque, 2002; Barth, 2007; Benaki et al., 1998; Berova, Polavarapu, Nakanishi, & Woody, 2012; Chaud et al., 2002; Eckert et al., 2016; Huang et al., 2011; Kaiden, Matsui, & Tanaka, 1987; Krimm & Bandekar, 1986; Lee et al., 2015; Mukherjee, Chowdhury, & Gai, 2007; Nakamoto, 2009; O'Loughlin et al., 2015; Prigogine & Rice, 2009; Trivedi & Vasudevan, 2007).

IR bands (wavenumber, cm^{-1})				Tentative assignment
H	F	R	WPI	
3437s, br	3427s, br	3432s, br	3411s, br	νO−H
3268vw	3268vw	–	3285s	Amide A (νN−H)
2967vw, 2927vw	2964vw, 2930vw	–	2960vw, 2927vw	νC$_{aliphatic}$−H
1632s	1632s	1632s	1632s	Amide I (νC=O)
1592s	1592s	1592s	1552w	Amide II
1385m, 1344w	1385m, 1344w	1385m, 1344w	1380m, 1344w	Amide III
1110w, 1039vw	1110w, 1039vw	1100vw, br	1110vw, br	νO−C
–	1077vw	–	1085vw	δC−H
–	989w	–	990w	νC−C−N
H−Fe C	**F−Fe C**	**R−Fe C**	**WPI−Fe C**	
3401s, br	3406s, br	3386s, br	3411s, br	νO−H
3268vw	3268vw	–	3272w	Amide A (νN−H)
3065w	3066w	–	3062w	νC$_{aromatic}$−H
2965, 2927vw	2964, 2932vw	–	2966, 2927vw	νC$_{aliphatic}$−H
1653s, br	1653s, br	1653s	1651s	Amide I + ν_{as}COO−Fe
1540m	1540m	1539s	1532w	Amide II
1431s	1431s	1431s	–	ν_sCOO−Fe
1344vw	1344vw	–	–	Amide III
1117vw	1117vw	1109vw	1114vw	νO−C−Fe
1073vw	1073vw	–	1070vw	δC−H
H−Fe S	**F−Fe S**	**R−Fe S**	**WPI−Fe S**	
3554sh, 3474sh, 3414s	3554sh, 3474sh, 3414s	3414s, br	3419s, br	νO−H + H-bonds
3248w	3248w	–	–	Amide A (νN−H)
2967,2927vw	2966, 2928vw	–	2968, 2927vw	νC$_{aliphatic}$−H
1640s, 1621w	1640s, 1619w	1641s	1641s	Amide I + ν_{as}COO−Fe
1556vw	1555vw	1543s	1542w	Amide II
1431vw	1431w	–	–	ν_sCOO−Fe
1385w	1385w	1385w	1380	Amide III
1146s	1150s	1149s	1144s	SO$_4^{2-}$
1114vw	1115vw	1122vw	1120vw	νO−C−Fe
993w	994vw	996w	–	νC−C−N
627m	624m	624w	619w	SO$_4^{2-}$

s = strong; br = broad; sh = shoulder; w = weak; vw = very weak; m = medium.

or ultrapure water were mixed with stock solutions of the ligands (7.5 mg protein/mL) to reach protein content of 5 mg/mL and iron:protein ratios of: 0, 10, 20, 30, 40, 60, 80, 100, 200, and 400 μmol Fe/g protein. After 5 min of iron addition, the fluorescence emission spectra were obtained as a plot of the fluorescence intensity versus wavelength (nm) (Lakowicz, 2006). Ten spectra were obtained for each ligand with different iron:protein ratios. All spectra were corrected for blank emission.

2.5. Synthesis of peptide-iron complexes and their iron-binding capacities

Hydrolysate (**H**) and its fractions **F** and **R** were used as ligands to synthesize the iron complexes. **WPI** was also studied as a ligand to compare the complexes synthesized with the whole protein. The iron precursor compounds were FeCl$_2$·4H$_2$O or FeSO$_4$·7H$_2$O. The reactions were conducted under the same conditions used in previous studies

(Caetano-Silva et al., 2015; Caetano-Silva et al., 2017) with an iron:protein ratio of 1:40 (w/w) and 1:5 (w/w), which is equivalent to 450 and 3600 μmol of Fe/g protein, respectively. The iron concentration was fixed at 0.1% (w/v), whereas the protein concentrations were 4% (w/v) and 0.5% (w/v). Briefly, ligand solutions were adjusted to pH 7.0 to favor deprotonation of the iron-binding sites (Porath, 1990), and the iron salt was added. The pH of each reaction medium was monitored and adjusted every 15 min. After 1 h of reaction with stirring (25 ± 2 °C), the suspensions were centrifuged (5000 g for 20 min) (Sorvall Instruments DuPont, RC5C, Wilmington, USA) and filtered through filter paper (Whatman n° 1). The iron content was determined in the supernatants via atomic absorption spectrophotometry (AAS) according to Boen, Soeiro, Pereira-Filho, and Lima-Pallone (2008) on a Perkin-Elmer Analyst 300 spectrometer (Norwalk, CT, USA) equipped with a deuterium lamp background corrector. Prior to iron determination, all samples were subjected to acid digestion with concentrated nitric acid and hydrogen peroxide (2:1 v/v) at 110 °C for 2 h and transferred quantitatively to volumetric flasks of 25 or 50 mL, and the volumes were completed with ultrapure water. All experiments were performed in triplicate. The iron content was measured using a hollow cathode lamp for iron (248.3 nm). The standard curve ranged from 0.2 to 2.6 mg Fe/L.

The iron-binding capacity (%) was calculated as the iron solubility in the supernatant with respect to the Fe initially added (Eq. (1)).

$$\text{Iron} - \text{binding capacity} (\%) = \frac{\text{Fe supernatant}}{\text{Fe initial}} \times 100 \qquad (1)$$

The supernatants containing the complexes were freeze-dried and stored frozen (− 18 °C). The iron complexes with **H**, **F**, **R**, and **WPI** were named **H−Fe**, **F−Fe**, **R−Fe**, and **WPI−Fe**, respectively. The iron source was expressed with the letters **C** or **S** for FeCl$_2$ or FeSO$_4$, respectively.

2.6. Characterization of the complexes

Ligands and ligand-iron complexes were analyzed via infrared (IR) spectroscopy. This technique is based on radiation absorption due to the vibration between molecular atoms (Haris & Chapman, 1995), and it has been used to obtain information about the chemical composition and conformational structure of proteins and peptides. Samples (2 mg) were mixed with dry KBr and compressed in a compact disc. The vibrational spectra were recorded on an FT-IR spectrometer (Nicolet iS5, Thermo Fisher Scientific, Waltham, MA, USA) in a spectral range from 4000 to 400 cm^{-1} with 32 scans and at a resolution of 2 cm^{-1}. Spectra were analyzed using the data analysis software, Origin 8.3 (Microcal Software, Inc., One Roundhouse Plaza, Northampton, MA, USA).

Ligand **F** and its respective complexes, **F−Fe C** and **F−Fe S**, were selected to be analyzed via thermal analyses concerning the influence of using different iron precursors. Thermogravimetry (TG) and differential thermal analysis (DTA) curves were obtained using a TA Instruments model SDTQ600 under a flow of dry synthetic air (150 mL min^{-1}), at a temperature up to 1000 °C, and at a heating rate of 10 °C min^{-1} in α-alumina sample holders.

2.7. Statistical analysis

The results of the iron determination were expressed as the means ± standard deviation and were statistically analyzed using the statistical package, GraphPad Prism 6 (GraphPad Software Inc., La Jolla, USA) via one-way analysis of variance (ANOVA). For significant differences between samples ($F_{calc} > F_{tab}$), the means were compared via post hoc Tukey's test. Values of $p < 0.05$ were considered to be significant.

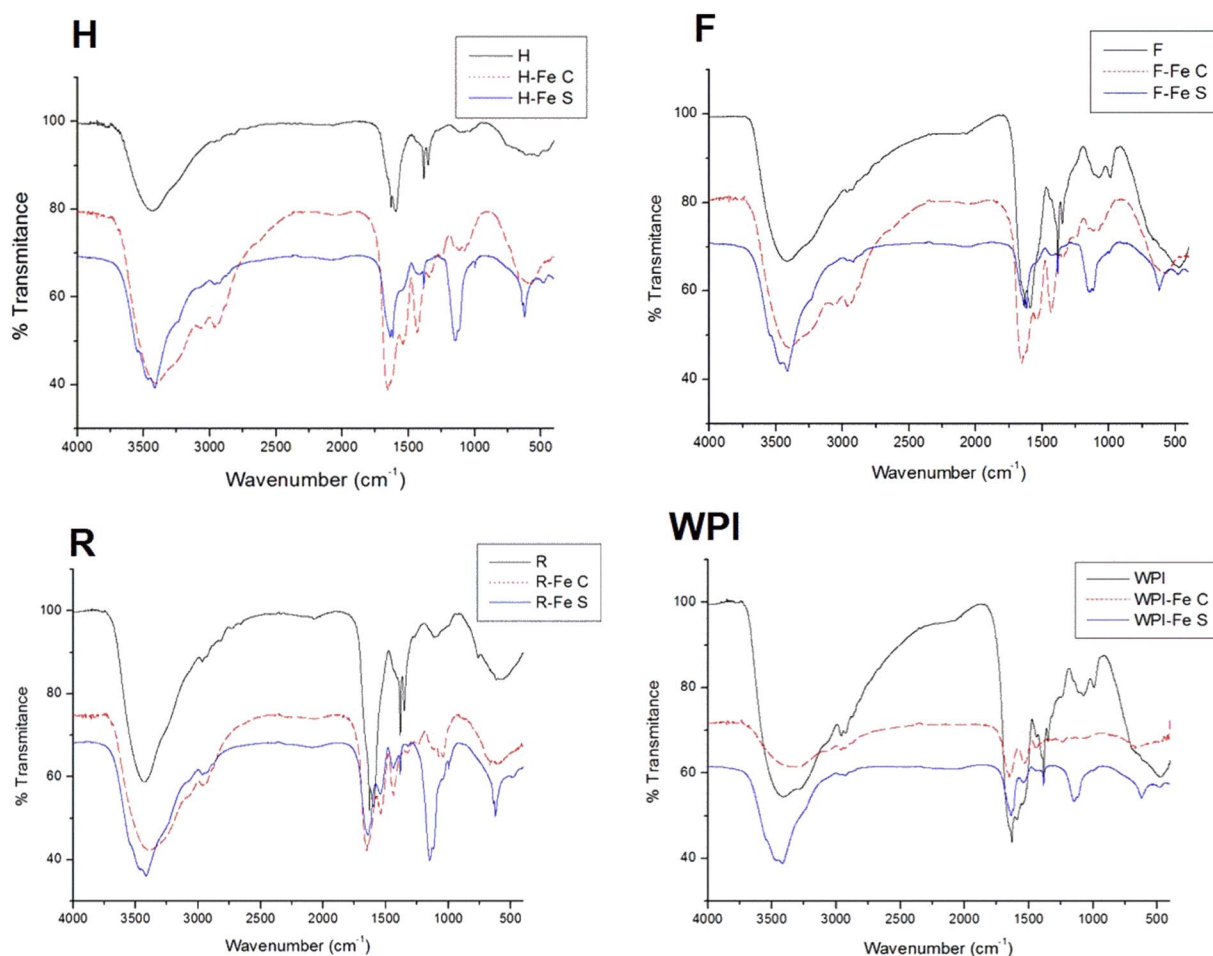**Fig. 4.** IR spectra of **H** - hydrolysate and its complexes (**H**−**Fe**); **F** - filtrate (fraction < 5 kDa) and its complexes (**F**−**Fe**); **R** - retentate (fraction > 5 kDa) and its complexes (**R**−**Fe**) and **WPI** – whey protein isolate and its complexes (**WPI**−**Fe**) synthesized from FeCl$_2$ (−**Fe C**) or FeSO$_4$ (−**Fe S**).

3. Results and discussion

3.1. Characterization of the ligands

The proteins, α-lactoalbumin (α-La) e β-lactoglobulin (β-Lg), were used as standards for RP-HPLC analysis, and showed retention times (RT) of 27.2 and 28.0 min, respectively. The chromatographic (RP-HPLC) profile of **H** and its fractions **F** and **R** (Fig. 1A) showed the absence of α-La and β-Lg peaks that were observed in the **WPI** profile, indicating that these proteins were hydrolyzed to smaller and more hydrophilic fragments. The profiles of **H** and **F** (Fig. 1A) are similar to each other, and the majority of peptides eluted in the high (RT < 10 min) and medium (10 min < RT < 20 min) hydrophilicity regions. On the other hand, the profile of **R** showed a lower number of peaks than the other ligands.

The electrophoretic (SDS-PAGE Tricine) profiles (Fig. 1B) showed differences in the MM values among the ligands. No band was observed in the profile of **F**, possibly due to the presence of peptides with an MM < 3 kDa, which were not dyed by Coomassie Blue (Krohn, 2001). The profile of **H** showed the disappearance of α-La (14.2 kDa) and β-Lg (18.4 kDa), which were both present in the **WPI** profile, due to the hydrolysis of these proteins to peptides of lower MM.

In the literature, there are some discrepancies regarding the iron-binding capacity of peptides with different MM values: the iron-binding capacity to peptides with a MM of 10–30 kDa (Lv et al., 2009) or to peptides with MM < 1 kDa (O'Loughlin et al., 2015) has been reported to be higher. The ligands showed differences in MM and hydrophilicity, which may lead to a different capacity of the free iron to access the

iron-binding sites, possibly resulting in different complexes.

3.2. Intrinsic fluorescence spectroscopy

The fluorescence emission spectra of the ligands with no addition of the iron salt and after the interaction with the metal in various concentrations (10, 20, 30, 40, 60, 80, 100, 200, and 400 μmol Fe/g protein) are shown in Fig. 2. The λ$_{max}$ of the ligands ranged from 310 to 350 nm, which is in accordance with the emission range of tryptophan (Trp) (Adams et al., 2002). The fluorescence emission spectra of **H** and the fractions **F** and **R** showed a higher intensity and a redshift of the λ$_{max}$ (λ$_{max}$ shifted to longer wavelengths) compared with the **WPI** spectra (Fig. 2 and Supplementary data, Table S1), suggesting that structural changes affected Trp upon hydrolysis (Zhou et al., 2012). The hydrolysis process yielded fragments with a lower MM and, as a result, a rearrangement occurred and the microenvironment of these residues could be changed. The fluorescence emission spectra of **H** and **F** showed differences in relation to the **R** spectra possibly due to differences in the peptide profiles, as observed in the chromatographic and electrophoretic profiles (Fig. 1).

The fluorescence intensity of all ligands at a fixed amount of protein (5 mg/mL) decreased up to 70% with iron addition regardless of the iron source. For all ligands, the highest iron:protein ratio (400 μmol Fe/g protein) led to the lowest fluorescence intensity. Iron interaction with iron-binding sites, especially carboxyl groups, may change Trp fluorescence depending on the impact of this interaction on the peptide/protein conformation (Lakowicz, 2006), since the Trp λ$_{max}$ and quantum yield (total intensity) are sensitive to the local electrostatic
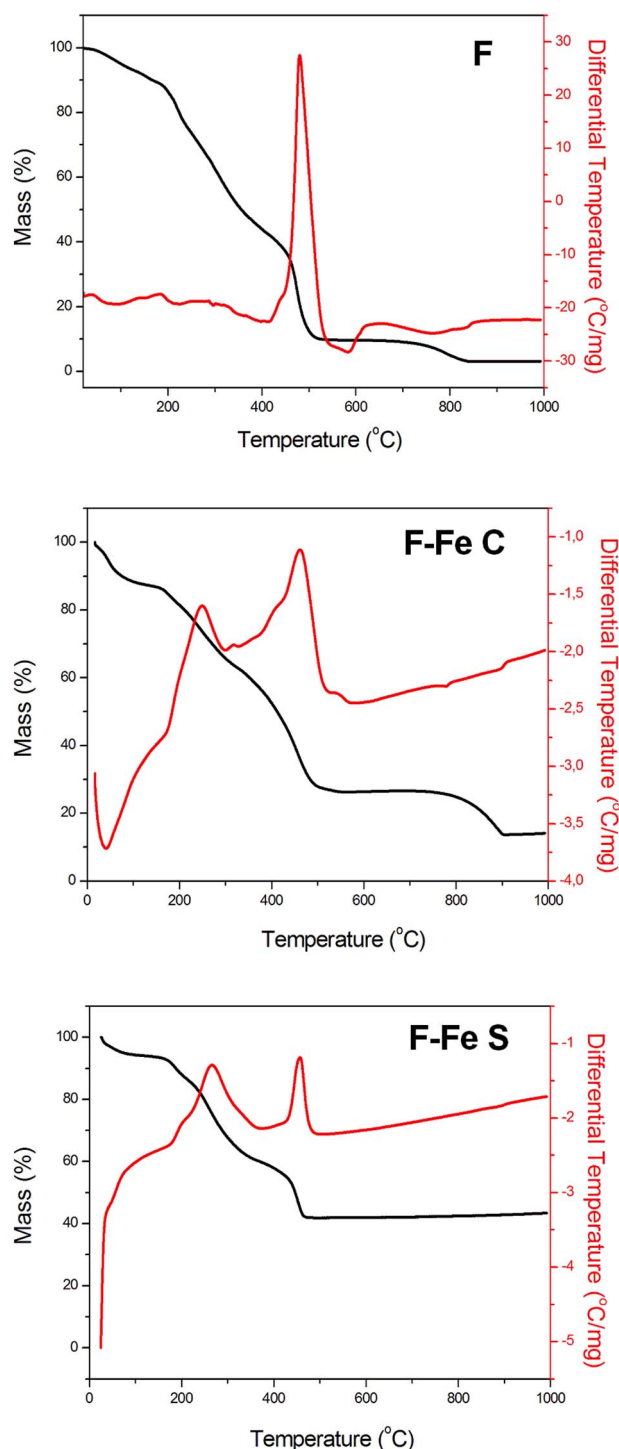
Fig. 5. TG and DTA curves of filtrate (fraction < 5 kDa) (**F**) and respective complexes synthesized with FeCl$_2$ (**F−Fe C**) or FeSO$_4$ (**F−Fe S**).

environment (Callis, 2014; Mach & Middaugh, 1994). The decrease in fluorescence intensity after iron addition may therefore be explained by the changes in peptide conformations as a consequence of iron-peptide interactions (Adams et al., 2002), which may transfer Trp residues to the surface of the molecule during complexation with iron (Zhou et al., 2012).

Other factors, such as ionic strength, may affect the conformation of the ligands (Dominy, Perl, Schmid, & Brooks, 2002) and interfere with their iron-binding capacity. The ionic strength of the reaction mixture increases up to 300% from 10 to 400 μmol Fe/g protein. At the same iron:protein ratio, the ionic strengths of reaction mixtures with FeSO$_4$ are approximately 30% higher than with FeCl$_2$. The salts affect the stability of proteins by modifying the ionic strength of the solution (Dominy et al., 2002), and they can exert specific effects on proteins that depend on the nature of the salt and its concentration, resulting in either stabilization or destabilization (Arakawa & Timasheff, 1984). The counter ions (SO$_4^{-2}$ and Cl$^-$) have different positions in the Hofmeister series (Zhang & Cremer, 2006), differing in their capacity to influence the protein stability and protein-protein interaction. The sulfate ion is larger than chloride and exerts an aggregation effect on proteins (salting out), whereas chloride ions exhibit a more solubilizing effect than SO$_4^{-2}$ (salting in) (Zhang & Cremer, 2006). Thus, the complexes could show differences regarding the conformation of peptides during their formation (*see the below Infrared discussion*).

3.3. Synthesis of peptide-iron complexes and their iron-binding capacities

Fig. 3 shows the iron-binding capacity expressed as iron solubility (%) at pH 7.0 after the synthesis of the complexes for both iron:protein ratios of 1:40 and 1:5. The low iron solubility observed in the control samples with iron salts (**BFe**) (1.5% for FeCl$_2$ and 18.4% for FeSO$_4$) is due to ferric hydroxide formation, which is insoluble at this pH. The synthesis reaction led to an increase in iron solubility, suggesting that all ligands exhibited an iron-binding capacity regardless of their MM, which is in accordance with the results obtained by other authors (Guo et al., 2013; Lv, Guo, Tako, & Glahn, 2014; Wu, Liu, Zhao, & Zeng, 2012). At a ratio of 1:40, complexes with FeCl$_2$ showed iron solubilities similar to those of FeSO$_4$ at 84 to 93%, which is possibly due to a large number of available iron-binding sites. At a ratio of 1:5, synthesis with FeCl$_2$ led to an iron solubility that was significantly higher than with FeSO$_4$, and led to greater differences among the ligands than with FeSO$_4$ (Fig. 3). The low iron solubility at this ratio ranging from 32% to 70% is related to the low peptide concentration of the synthesis mixture in relation to the iron concentration and the consequent low availability of iron-binding sites. At this ratio, pH instability of the reaction medium was observed (7.0 to 5.8 in 15 min). This pH drop during the synthesis reaction may have changed the protonated state of the iron-binding sites, hindering the iron interaction with the peptides. Therefore, part of the iron ions formed FeOH.

3.4. Characterization of the complexes

The IR spectra of the complexes synthesized with an iron:protein ratio of 1:40 showed no detectable difference from the spectra of the corresponding free ligand (data not shown). The high proportion of unbound peptides may have overlapped shifts induced by iron binding, hindering the observation of relevant information. Spectra of the complexes synthesized with an iron:protein ratio of 1:5 enabled IR spectral evaluation due to the differences observed in relation to the spectra of the free ligands.

Table 1 shows the main absorption bands in the infrared spectra and the assignments of the corresponding vibrational modes of the free ligands and the peptide-iron complexes.

Concerning the free ligands, several differences were observed in the vibrational spectrum of **WPI** in relation to **H**, **F**, and **R**. For instance, the Amide II band can be observed as a strong band at 1592 cm^{-1} in the spectra of the peptide ligands (**H**, **F**, and **R**) and at 1552 cm^{-1} in the **WPI** spectrum (Prigogine & Rice, 2009) (Table 1). The Amide II band shows the breaking of peptide bonds during the hydrolysis process since this band is dependent on secondary conformations, and its position for intact protein and peptides is different (Prigogine & Rice, 2009).

Regardless of the iron precursor compound (FeCl$_2$ or FeSO$_4$) or the ligand, in general, the interactions of the divalent metallic ion and the ligands led to the formation of orange species, which is the characteristic color of iron(III) compounds. The synthesis reaction conditions lead to the conversion of ferrous to the ferric form due to the presence

Table 2

Initial and final temperatures (°C), partial mass losses (%), and DTA peaks (°C) of filtrate (**F**) and the corresponding peptide-iron complexes, **F−Fe C** and **F−Fe S**.

Compound	Step	ΔT (°C)	Δm (%)	DTA peaks (°C)		Assignments
				Endo	Exo	
F	1	22–417	57.4	83.5	183.4	Water evaporation and combustion
	2	417–558	32.2	–	480.4	Sample decomposition from rupture of polypeptide bonds, forming carbonaceous material
	3	558–876	7.0	–	–	Decomposition of carbonaceous material
F−Fe C	1	17–118	12.4	40.4	–	Water evaporation
	2	118–331	24.9	170.4	249.1	Coordinated water liberation and rupture of peptide-Fe bonds
	3	331–577	35.7	–	461.9	Rupture of polypeptide bonds and formation of Fe_2O_3
	4	761–906	13.3	–	–	Decomposition of carbonaceous material
F−Fe S	1	25–156	6.6	42.6	–	Water evaporation
	2	156–348	31.8	171.5	265.1	Coordinated water liberation and rupture of peptide-Fe bonds
	3	348–476	19.3	–	456.6	Rupture of polypeptide bonds and formation of Fe_2O_3

F: free ligand, filtrate (fraction < 5 kDa); **F−Fe C**: peptide-iron complex synthesized with filtrate (fraction < 5 kDa) and $FeCl_2$; **F−Fe S**: peptide-iron complex synthesized with filtrate (fraction < 5 kDa) and $FeSO_4$.
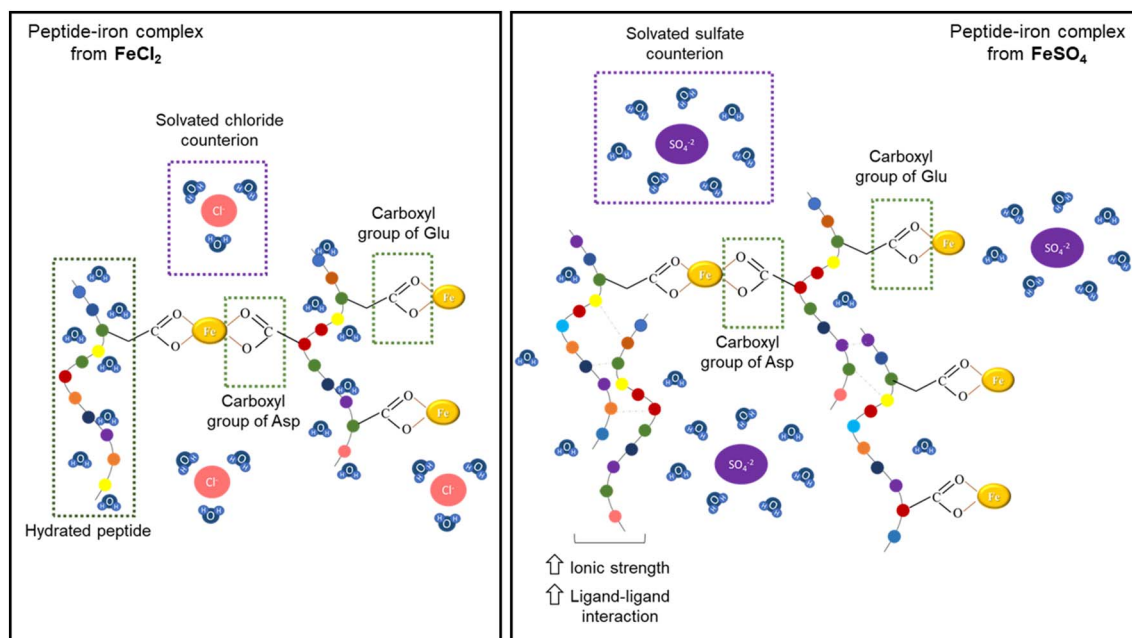
Fig. 6. Simplified model of peptide-iron complexes.

of oxygen. This conversion may favor the formation of the complexes, since, as a hard acid, Fe^{3+} forms high-affinity complexes with hard oxygen ligands as carboxyl groups. Thus, the thermodynamic preference of these groups can be for Fe^{3+} instead of for di-cationic metal ions (Haas & Franz, 2009), which suggests that the majority of the complexes were formed with iron ions in the ferric form.

Both IR and TG/DTA techniques were used to characterize the peptide-iron complexes and allowed inference of some important aspects, which are divided into two main topics: (I) iron coordination by the ligands and (II) the influence of the iron precursor compounds, which will be discussed in detail.

(I) Iron coordination by the ligands

The Amide I band is originated primarily from the peptide C=O stretching vibration mode and was observed at 1632 cm^{-1} (Mukherjee et al., 2007) in the free ligand spectra (Table 1). After complexation, it was split into two components in the spectra of both $FeSO_4$ and $FeCl_2$ complexes (Fig. 4). The second component corresponds to the asymmetric stretching of the Fe−COO bond (near 1620 cm^{-1}) (Trivedi & Vasudevan, 2007), confirming the formation of iron complexes through the interaction with the carboxyl group preferentially

with the side chains of Asp or Glu residues.

At 1431 cm^{-1}, for the complexes with both iron sources, the appearance of an important band associated with the symmetric stretching vibration of the Fe−COO bond (Acevedo-Chávez et al., 2002) was observed. In addition, the shift in the ν_sC−O bands from 1110–1039 (**H** and **F**) to 1117 cm^{-1} in the complexes indicates the formation of Fe−O−C bonds (Chaud et al., 2002; Huang et al., 2011). However, for the complexes obtained with $FeSO_4$, the real value cannot be observed from the IR spectra because sulfate overlaps the band in the same region (the sulfate vibrational mode is a very intense band at 1146–1150 cm^{-1}) (Nakamoto, 2009). O'Loughlin et al. (2015) also observed a band at 1110 cm^{-1}, which was assigned to a sulfate group in a fraction of whey hydrolysate added to $FeSO_4$. Thus, much information concerning the metal-peptide interaction in $FeSO_4$ complexes could be hidden under this broad band. The sulfate group is an integral part of the Fe complexes, either in the coordinated form, [Fe(pept)SO$_4$], or as a counter ion, [Fe(pept)]SO$_4$.

Despite the differences in the MM profile of the ligands (Fig. 1), it was possible to infer metal coordination with all ligands and their iron-binding sites seem to be the same. High MM peptides (ligand **R**) or the structure of the whole protein (**WPI**) did not impair the linkage with iron atoms. In fact, in a previous work (Caetano-Silva et al., 2015), we

demonstrated that the iron-binding peptides are similar in both types of fractions (**F** and **R**). The fragments, which are rich in the main iron-binding sites in the Asp (D) and Glu (E) residues (Chaud et al., 2002; Lv et al., 2009), were from the sequences [42]YVEELKPTPEGDLEIL[57] and [124]RTPEVDDEALEK[135] from β-Lg and [82]DDDLTDDI[89] from α-La. However, it is not possible to quantify the coordinate covalent bonds formed in those different complexes. Besides the coordinate covalent bond, other interactions, such as Van der Waals forces, hydrophobic forces, and hydrogen bonding, strongly influence the peptide-Fe complex formation and even its stability (Eckert et al., 2016; Faa & Crisponi, 1999). The differences in the complexes synthesized with different ligands may be related to the differences in in vitro iron absorption observed in a previous work (Caetano-Silva et al., 2017).

(II) Influence of the iron precursor compounds

Concerning the different iron precursor compounds, $FeCl_2$ or $FeSO_4$, the infrared spectroscopy also allowed identification of significant differences among the obtained complexes. The IR spectra of the free ligands (**H**, **F**, **R**, and **WPI**), as illustrated in Fig. 4, show two components of the Amide III band at 1385 cm^{-1} (band of medium intensity) and 1344 cm^{-1} (weak band) (Benaki et al., 1998) (see also Table 1). This band involves a combination of peptide N−H in-plane bending and C−N stretching motions, and it is conformationally sensitive (Kaiden et al., 1987). IR spectra of the complexes with $FeSO_4$ showed the most important component of the Amide III band (1385 cm^{-1}), whereas in the IR spectra of the peptide-Fe complexes formed from $FeCl_2$, only the second component (at 1344 cm^{-1}) can be observed, which can be tentatively assigned to the presence of hydrated α-helix (Berova et al., 2012). This result is in accordance with the presence of an intense and broad νO−H band at 3401 cm^{-1} in the spectra of $FeCl_2$ complexes assigned to water molecule vibrations. These spectroscopic results suggest a strong local structural distortion in the $FeCl_2$ complexes as a result of the coordination (Haris & Chapman, 1995; Ianoul, Boyden, & Asher, 2001).

The Amide A band, which is assigned to the stretching vibration of the N−H bond (Barth, 2007), was observed in the spectra of the $FeCl_2$ complexes in the same region as that of the free ligands (3268 cm^{-1}, Table 1), suggesting that iron was not coordinated with the amino groups in these compounds. The pH of the reaction (7.0) was lower than the pKa of the NH_3^+ group (~9.5); thus, the majority of amino groups was protonated during the synthesis. This fact possibly hindered the formation of Fe−N bonds. The same occurred with the complexes with $FeSO_4$, which is in accordance with Eckert et al. (2016), who also reported that Fe^{2+} did not bind to the N-terminus of a heptapeptide from barley protein. However, in the $FeSO_4$ complexes, the Amide A band exhibited a shift towards a lower wavenumber (from 3268 in free ligand to 3248 cm^{-1}), suggesting an increase in hydrogen bond forces (Barth, 2007), since this band is very sensitive to the strength of hydrogen bonds (Krimm & Bandekar, 1986). Analyzing the region associated with the O−H stretching vibrational modes, besides the main band at 3414 cm^{-1}, very weak bands at 3554 and 3474 cm^{-1}, which were assigned to H-bonds (Lee et al., 2015), were observed in the spectra of the $FeSO_4$ complexes but not in the $FeCl_2$ complexes. Therefore, $FeSO_4$ complexes seem to present more hydrogen bonds than the $FeCl_2$ ones as a result of ligand-ligand interactions. This finding can be explained by the greater effect exerted by sulfate anions towards protein aggregation, which is in strong agreement with the difference in position of these ions in the Hofmeister series, as discussed earlier.

Concerning the TG and DTA curves, the complexes, **F**−**Fe C** and **F**−**Fe S**, showed different thermal behaviors (Fig. 5), corroborating the IR results. The curve of the free ligand (**F**) showed the same global trend reported in the literature as the thermal behavior of the proteins (Dandurand et al., 2014; Zhang et al., 2016). The peptide-Fe complex obtained from $FeCl_2$ (**F**−**Fe C**) decomposed in three steps after the dehydration process occurred between 17 and 118 °C, whereas the

thermal decomposition of **F**−**Fe S** occurred in only two steps after the evaporation of adsorbed water was observed in the range of 25–156 °C (with corresponding weight loss of 6.6%) (Fig. 5). The water loss of **F**−**Fe C** (12.4%) was approximately 88% higher than the **F**−**Fe S**, which is consistent with the IR spectroscopic studies that revealed the presence of hydrated α-helix in the complexes obtained from $FeCl_2$ and an intense and broad νO−H band at 3401 cm^{-1}, which was assigned to water molecule vibrations (see Fig. 4).

For both complexes, step 2 (Table 2) is most likely related to the removal of coordinated water and the rupture of the peptide-iron bond, accompanied by DTA exothermic peaks at 249.1 and 265.1 °C for **F**−**Fe C** and **F**−**Fe S**, respectively. The breaking of the peptide bonds (Table 2) corresponded to the final loss of the remaining organic part, accompanied by the formation of Fe_2O_3 as the final product. For the **F**−**Fe C** complex, however, one more step was observed in which the carbonaceous material slowly decomposed at a temperature from 761 to 906 °C.

It is evident, therefore, that the distinct spectroscopic and thermal behaviors of **F**−**Fe S** and **F**−**Fe C** allowed inferring that the counter ions, which influenced the ligand-metal and ligand-ligand interactions, play a crucial role in the complex structure and its potential biological activity. Different structures can lead to different exposure of cleavage sites of gastrointestinal enzymes, which can subsequently influence the complexes digestion and iron uptake (Caetano-Silva et al., 2017; Eckert et al., 2016).

3.5. Simplified model of peptide-iron complexes

Fig. 6 shows a simplified model of the peptide-iron complexes, which was outlined based on our results. Other authors have also found carboxyl groups as the main iron-binding sites during the formation of peptide-iron complexes (Chaud et al., 2002; Huang et al., 2011; O'Loughlin et al., 2015; Sun et al., 2017; Zhou et al., 2012). The schematic diagram (Fig. 6) highlights the main iron linkage with the carboxyl groups via bidentate coordination and the influence of the counter ions on the ligand conformation, which results in different complexes.

4. Conclusions

Complexes synthesized from both iron precursor compounds, $FeCl_2$ and $FeSO_4$, showed metal-carboxylate coordination via the bidentate mode and different effects on the ligand conformation. The counter ions play a central role in the process of complex formation, since they may interfere either in the exposure of binding sites of the peptides or in the complex conformations. In fact, chloride or sulfate substantially affects the dynamic of peptide-Fe interaction, yielding entirely different compounds.

The adequate choice for the iron source to synthesize peptide-iron complexes may be of great importance since ligand conformation and complexes structure can lead to differences in iron absorption. Future studies may evaluate the influence of different iron precursors on the iron pro-oxidant capacity and its interaction with other compounds.

Supplementary data to this article can be found online at http://dx.doi.org/10.1016/j.foodres.2017.08.056.

References

Acevedo-Chávez, R., Costas, M. E., Bernès, S., Medina, G., & Gasque, L. (2002). A ferri-magnetic cyclic tetranuclear copper (II) complex: Cyclo-[tetrakis (μ-η3-hydro-xyethanoato-1κ O:2κ2O′,O″)tetrakis(1,10-phenanthroline)tetracopper]tetranitrate dihydrate. Structural and magnetic properties. *Journal of the Chemical Society, Dalton Transactions, 12*, 2553–2558.

Adams, P. D., Chen, Y., Ma, K., Zagorski, M. G., Sönnichsen, F. D., McLaughlin, M. L., & Barkley, M. D. (2002). Intramolecular quenching of tryptophan fluorescence by the peptide bond in cyclic hexapeptides. *Journal of the American Chemical Society, 124*(31), 9278–9286.

Adler-Nissen, J. (1986). *Enzymic hydrolysis of food proteins.* New York: Elsevier Applied Science Publishers.

Arakawa, T., & Timasheff, S. N. (1984). Mechanism of protein salting in and salting out by divalent cation salts: Balance between hydration and salt binding. *Biochemistry, 23*(25), 5912–5923.

Barth, A. (2007). Infrared spectroscopy of proteins. *Biochimica et Biophysica Acta - Bioenergetics, 1767*(9), 1073–1101.

Benaki, D. C., Aggeli, A., Chryssikos, G. D., Yiannopoulos, Y. D., Kamitsos, E. I., Brumley, E., ... Hamodrakas, S. J. (1998). Laser-raman and FT-IR spectroscopic studies of peptide-analogues of silkmoth chorion protein segments. *International Journal of Biological Macromolecules, 23*(1), 49–59.

Berova, N., Polavarapu, P. L., Nakanishi, K., & Woody, R. W. (2012). In J. W. Sons (Vol. Ed.), *Comprehensive chiroptical spectroscopy, applications in stereochemical analysis of synthetic compounds, natural products, and biomolecules. Vol. 2.*

Boen, T. R., Soeiro, B. T., Pereira-Filho, E. R., & Lima-Pallone, J. A. (2008). Folic acid and iron evaluation in Brazilian enriched corn and wheat flours. *Journal of the Brazilian Chemical Society, 19*, 53–59.

Caetano-Silva, M. E., Bertoldo-Pacheco, M. T., Paes-Leme, A. F., & Netto, F. M. (2015). Iron-binding peptides from whey protein hydrolysates: Evaluation, isolation and sequencing by LC-MS/MS. *Food Research International, 71*, 132–139.

Caetano-Silva, M. E., Cilla, A., Bertoldo-Pacheco, M. T., Netto, F. M., & Alegría, A. (2017). Evaluation of in vitro iron bioavailability in free form and as whey peptide-iron complexes. *Journal of Food Composition and Analysis.* http://dx.doi.org/10.1016/j.jfca.2017.03.010.

Callis, P. R. (2014). Binding phenomena and fluorescence quenching. Ii: Photophysics of aromatic residues and dependence of fluorescence spectra on protein conformation. *Journal of Molecular Structure, 1077*, 22–29.

Chaud, M. V., Izumi, C., Nahaal, Z., Shuhama, T., Bianchi Mde, L., & de Freitas, O. (2002). Iron derivatives from casein hydrolysates as a potential source in the treatment of iron deficiency. *Journal of Agricultural and Food Chemistry, 50*(4), 871–877.

Dandurand, J., Samouillan, V., Lacoste-Ferre, M. H., Lacabanne, C., Bochicchio, B., & Pepe, A. (2014). Conformational and thermal characterization of a synthetic peptidic fragment inspired from human tropoelastin: Signature of the amyloid fibers. *Pathologie Biologie (Paris), 62*(2), 100–107.

Dominy, B. N., Perl, D., Schmid, F. X., & Brooks, C. L. (2002). The effects of ionic strength on protein stability: The cold shock protein family. *Journal of Molecular Biology, 319*(2), 541–554.

Eckert, E., Lu, L., Unsworth, L. D., Chen, L., Xie, J., & Xu, R. (2016). Biophysical and in vitro absorption studies of iron chelating peptide from barley proteins. *Journal of Functional Foods, 25*, 291–301.

Faa, G., & Crisponi, G. (1999). Iron chelating agents in clinical practice. *Coordination Chemistry Reviews, 184*(1), 291–310.

Gligic, L., Palic, T., & Nikolovski, J. (2004). The beneficial effects of iron-enriched yeast *Saccharomyces cerevisiae* biomass in poultry breeding. *Folia Veterinaria, 48*(2), 104–107.

Guo, L., Hou, H., Li, B., Zhang, Z., Wang, S., & Zhao, X. (2013). Preparation, isolation and identification of iron-chelating peptides derived from Alaska pollock skin. *Process Biochemistry, 48*(5–6), 988–993.

Haas, K. L., & Franz, K. J. (2009). Application of metal coordination chemistry to explore and manipulate cell biology. *Chemical Reviews, 109*(10), 4921–4960.

Haris, P. I., & Chapman, D. (1995). The conformational analysis of peptides using Fourier transform IR spectroscopy. *Biopolymers, 37*(4), 251–263.

Huang, G., Ren, Z., & Jiang, J. (2011). Separation of iron-binding peptides from shrimp processing by-products hydrolysates. *Food and Bioprocess Technology, 4*(8), 1527–1532.

Ianoul, A., Boyden, M. N., & Asher, S. A. (2001). Dependence of the peptide amide III vibration on the φ dihedral angle. *Journal of the American Chemical Society, 123*(30), 7433–7434.

Kaiden, K., Matsui, T., & Tanaka, S. (1987). A study of the amide III band by FT-IR

spectrometry of the secondary structure of albumin, myoglobin, and γ-globulin. *Applied Spectroscopy, 41*(2), 180–184.

Kim, S. B., Seo, I. S., Khan, M. A., Ki, K. S., Nam, M. S., & Kim, H. S. (2007). Separation of iron-binding protein from whey through enzymatic hydrolysis. *International Dairy Journal, 17*(6), 625–631.

Krimm, S., & Bandekar, J. (1986). Vibrational spectroscopy and conformation of peptides, polypeptides, and proteins. In C. B. Anfinsen, J. T. Edsall, & F. M. Richards (Vol. Eds.), *Advances in protein chemistry. Vol. 38. Advances in protein chemistry* (pp. 181–364). Academic Press.

Krohn, R. I. (2001). *The colorimetric detection and quantitation of total protein. Current protocols in cell biology.* John Wiley & Sons, Inc.

Lakowicz, J. R. (2006). *Principles of fluorescence spectroscopy.* New York: Springer.

Lee, C. M., Kubicki, J. D., Fan, B., Zhong, L., Jarvis, M. C., & Kim, S. H. (2015). Hydrogen-bonding network and OH stretch vibration of cellulose: Comparison of computational modeling with polarized iIR and SFG spectra. *The Journal of Physical Chemistry B, 119*(49), 15138–15149.

Lieu, P. T., Heiskala, M., Peterson, P. A., & Yang, Y. (2001). The roles of iron in health and disease. *Molecular Aspects of Medicine, 22*(1–2), 1–87.

Luo, Y., & Xie, W. (2012). Effect of phytase treatment on iron bioavailability in faba bean (Vicia faba l.) flour. *Food Chemistry, 134*(3), 1251–1255.

Lv, Y., Guo, S., Tako, E., & Glahn, R. P. (2014). Hydrolysis of soybean protein improves iron bioavailability by Caco-2 cell. *Journal of Food and Nutrition Research, 2*(4), 162–166.

Lv, Y., Liu, Q., Bao, X., Tang, W., Yang, B., & Guo, S. (2009). Identification and characteristics of iron-chelating peptides from soybean protein hydrolysates using IMAC-Fe^{3+}. *Journal of Agricultural and Food Chemistry, 57*(11), 4593–4597.

Mach, H., & Middaugh, C. R. (1994). Simultaneous monitoring of the environment of tryptophan, tyrosine, and phenylalanine residues in proteins by near-ultraviolet second-derivative spectroscopy. *Analytical Biochemistry, 222*(2), 323–331.

Miquel, E., & Farré, R. (2007). Effects and future trends of casein phosphopeptides on zinc bioavailability. *Trends in Food Science & Technology, 18*(3), 139–143.

Mukherjee, S., Chowdhury, P., & Gai, F. (2007). Infrared study of the effect of hydration on the amide I band and aggregation properties of helical peptides. *The Journal of Physical Chemistry B, 111*(17), 4596–4602.

Nakamoto, K. (2009). *Infrared and Raman spectra of inorganic and coordination compounds part a: Theory and applications in inorganic chemistry* (6 ed.). New Jersey: John Wiley and Sons.

O'Loughlin, I. B., Kelly, P. M., Murray, B. A., FitzGerald, R. J., & Brodkorb, A. (2015). Molecular characterization of whey protein hydrolysate fractions with ferrous chelating and enhanced iron solubility capabilities. *Journal of Agricultural and Food Chemistry, 63*(10), 2708–2714.

Porath, J. (1990). Amino acid side chain interaction with chelate-liganded crosslinked dextran, agarose and TSK gel. A mini review of recent work. *Journal of Molecular Recognition, 3*(3), 123–127.

Prigogine, I., & Rice, S. A. (2009). In J. W. Sons (Vol. Ed.), *Advances in chemical physics. Vol. 111.*

Schagger, H. (2006). Tricine-SDS-PAGE. *Nature Protocols, 1*(1), 16–22.

Sugiarto, M., Ye, A., & Singh, H. (2009). Characterisation of binding of iron to sodium caseinate and whey protein isolate. *Food Chemistry, 114*(3), 1007–1013.

Sun, N., Cui, P., Jin, Z., Wu, H., Wang, Y., & Lin, S. (2017). Contributions of molecular size, charge distribution, and specific amino acids to the iron-binding capacity of sea cucumber (*Stichopus japonicus*) ovum hydrolysates. *Food Chemistry, 230*, 627–636.

Trivedi, P., & Vasudevan, D. (2007). Spectroscopic investigation of ciprofloxacin speciation at the goethite-water interface. *Environmental Science & Technology, 41*(9), 3153–3158.

Ueno, H. M., Urazono, H., & Kobayashi, T. (2014). Serum albumin forms a lactoferrin-like soluble iron-binding complex in presence of hydrogen carbonate ions. *Food Chemistry, 145*(0), 90–94.

Wu, H., Liu, Z., Zhao, Y., & Zeng, M. (2012). Enzymatic preparation and characterization of iron-chelating peptides from anchovy (*Engraulis japonicus*) muscle protein. *Food Research International, 48*(2), 435–441.

Zhang, H., Frey, M., Navizaga, C., Lenzo, C., Taborda, J., Taifan, W., ... Baltrusaitis, J. (2016). Dairy wastewater for production of chelated biodegradable Zn micronutrient fertilizers. *ACS Sustainable Chemistry & Engineering, 4*(3), 1722–1727.

Zhang, Y., & Cremer, P. S. (2006). Interactions between macromolecules and ions: The Hofmeister series. *Current Opinion in Chemical Biology, 10*(6), 658–663.

Zhou, J., Wang, X., Ai, T., Cheng, X., Guo, H. Y., Teng, G. X., & Mao, X. Y. (2012). Preparation and characterization of β-lactoglobulin hydrolysate-iron complexes. *Journal of Dairy Science, 95*(8), 4230–4236.